

## EVIDENCE FOR GRAVITATIONAL INFALL OF MATTER ONTO THE SUPERMASSIVE BLACK HOLE IN THE QUASAR PG 1211+143?

J. N. REEVES,<sup>1,2</sup> K. POUNDS,<sup>3</sup> P. UTTLEY,<sup>1</sup> S. KRAEMER,<sup>1,4</sup> R. MUSHOTZKY,<sup>1</sup> T. YAQOOB,<sup>1,2</sup> I. M. GEORGE,<sup>1,5</sup> AND T. J. TURNER<sup>1,5</sup>

Received 2005 August 1; accepted 2005 October 5; published 2005 October 27

### ABSTRACT

We report the detection of redshifted iron  $K\alpha$  absorption lines in the *Chandra* LETG spectrum of the narrow-line quasar PG 1211+143. The absorption lines are observed at 4.22 and 4.93 keV in the quasar spectrum, corresponding to 4.56 and 5.33 keV in the rest frame of PG 1211+143. From Monte Carlo simulations, the chance probability of both lines being false detections is low at  $1.36 \times 10^{-4}$ . Highly redshifted ionized iron  $K\alpha$  (Fe xxv or Fe xxvi) is the most plausible identification for the lines at their observed energies. If identified with H-like iron  $K\alpha$  at 6.97 keV, then the relativistic velocity shifts required are  $0.40c$  and  $0.26c$ . The extreme velocities can be explained by pure gravitational redshift if the matter exists in a stable orbit within 6 gravitational radii of the black hole. This would require a Kerr metric for the black hole. Alternatively, the absorption may be the result of matter infalling directly onto the black hole, with a maximum observed velocity of  $0.38c$  at  $6R_g$  in the Schwarzschild metric. This matter may originate in a failed outflow or jet, which does not escape the gravitational potential of the black hole.

*Subject headings:* black hole physics — quasars: individual (PG 1211+143) — X-rays: galaxies

*Online material:* color figures

### 1. INTRODUCTION

One prime motivation for high-energy research into active galactic nuclei (AGNs) is to find evidence of the putative massive black hole, through the gravitational redshift imparted on photons emerging within a few gravitational radii of the event horizon. To date, most of the effort has focused on the iron  $K\alpha$  emission line, predicted to show a relativistically broadened profile (Fabian et al. 1989; Laor 1991), which appeared to be common among Seyfert 1 galaxies, as observed by *ASCA* (Tanaka et al. 1995; Nandra et al. 1997). However, the situation emerging from the newer *XMM-Newton* and *Chandra* data is more ambiguous, with the spectra showing that narrower (non-relativistic) lines are commonplace (Yaqoob & Padmanabhan 2004). Indeed, the red wing of the broad iron line is often hard to distinguish from the effects of the warm absorber (Reeves et al. 2004; Turner et al. 2005a).

Narrow, transient, and redshifted iron emission lines of modest statistical significance have recently been claimed in several AGNs (Turner et al. 2002; Dovciak et al. 2004; Porquet et al. 2004), possibly originating from local hot spots on the disk surface. Potentially, these lines can be tracked to reveal orbital motions in the inner disk (Dovciak et al. 2004; Turner et al. 2005b). However, little evidence has been found to date for infall of matter onto the black hole. In this Letter, we present evidence of highly redshifted iron  $K\alpha$  absorption lines in the narrow-line Seyfert 1 galaxy PG 1211+143 (at  $z = 0.0809$ ) using the Low Energy Transmission Grating (LETG) on *Chandra*. This may be interpreted either as infall onto the massive

black hole or as a gravitational redshift occurring within  $<6R_g$  of a Kerr black hole. A previous *XMM-Newton* observation of PG 1211+143 showed blueshifted absorption from a high-velocity ( $v \sim 0.1c$ ) outflow (Pounds et al. 2003). The soft X-ray properties of PG 1211+143, which confirm the blueshifted absorber, will be presented in a subsequent paper. Values of  $H_0 = 70 \text{ km s}^{-1} \text{ Mpc}^{-1}$ ,  $q_0 = 0.0$ , and  $\Lambda_0 = 0.73$  are assumed, and errors are quoted at 90% confidence ( $\Delta\chi^2 = 2.7$ ), for one parameter of interest.

### 2. CHANDRA AND XMM-NEWTON OBSERVATIONS OF PG 1211+143

PG 1211+143 was observed by *Chandra* with the LETG in three consecutive orbits between 2004 June 21 and 26 of approximately 45 ks exposure per orbit (see Table 1). An *XMM-Newton* observation was conducted simultaneously with the first *Chandra* orbit, but due to high and variable background, this was reduced to only  $\sim 20$  ks of useful exposure. The ACIS-S detector was used on the focal plane, with the S3 chip being at the telescope aim point. *Chandra* LETG source spectra, background spectra, and response matrices were generated using CIAO 3.2.1. Streaks were removed from the ACIS-S CCD array, while events with grades 0, 2, 3, 4, and 6 were selected. After screening, an exposure of 133.6 ks was obtained. Spectra and responses from the  $\pm 1$  orders were extracted and combined to maximize the signal-to-noise ratio. The time-averaged combined first-order LETG count rate was  $0.31 \text{ counts s}^{-1}$ . The first-order spectra were binned so that one bin represents the FWHM resolution of the LETG ( $\Delta\lambda = 0.05$ ), ensuring sufficient counts per bin to use the  $\chi^2$  minimization spectral fitting technique.

### 3. LETG SPECTRAL ANALYSIS

To parameterize the X-ray continuum, the LETG spectrum was fitted with a broken power-law model, modified by neutral Galactic absorption of  $N_H = 2.8 \times 10^{20} \text{ cm}^{-2}$  (Dickey & Lockman 1990), over the 0.4–8.0 keV bandpass. The soft and hard X-ray photon indices, break energy, and model normalization were allowed to vary; the best-fit values are  $\Gamma_{\text{soft}} = 2.77 \pm 0.03$ ,  $\Gamma_{\text{hard}} = 1.96 \pm 0.05$ , break energy  $E = 1.7 \pm 0.1 \text{ keV}$ , and a normalized flux of  $(1.6 \pm 0.1) \times 10^{-3} \text{ photons keV}^{-1}$

<sup>1</sup> Exploration of the Universe Division, NASA Goddard Space Flight Center, Greenbelt Road, Greenbelt, MD 20771; jnr@milkyway.gsfc.nasa.gov, pu@milkyway.gsfc.nasa.gov, richard@milkyway.gsfc.nasa.gov.

<sup>2</sup> Department of Physics and Astronomy, Johns Hopkins University, Charles and 34th Street, Baltimore, MD 21218-2686; yaqoob@skysrv.pha.jhu.edu.

<sup>3</sup> Department of Physics and Astronomy, University of Leicester, University Road, Leicester LE1 7RH, UK; kap@star.le.ac.uk.

<sup>4</sup> Department of Physics, Catholic University of America, 620 Michigan Avenue, NE, Washington, DC 20064; stiskraemer@yancey.gsfc.nasa.gov.

<sup>5</sup> Joint Center for Astrophysics, University of Maryland Baltimore County, 1000 Hilltop Circle, Baltimore, MD 21250; george@milkyway.gsfc.nasa.gov, turner@milkyway.gsfc.nasa.gov.

TABLE 1  
IRON LINE SPECTRAL FITS

Parameter	Mean	Obs. 1	Obs. 2	Obs. 3
Start date (2004) .....	Jun 21	Jun 21	Jun 23	Jun 25
Start time (UT) .....	03:09:04	03:09:04	03:57:43	18:30:27
Exposure time (ks) .....	133.6	42.7	48.2	42.7
$\Gamma^a$ .....	$1.99 \pm 0.06$	$1.87 \pm 0.14$	$2.00 \pm 0.10$	$1.93 \pm 0.10$
$F_{2-10 \text{ keV}}^b$ ( $10^{-12}$ ergs $\text{cm}^{-2}$ $\text{s}^{-1}$ ) .....	6.1	4.0	6.6	7.3
Energy <sup>c</sup> (keV) .....	$4.22 \pm 0.03$	$4.22^d$	$4.22 \pm 0.03$	$4.22^d$
	$4.93 \pm 0.03$	$4.93^d$	$4.89 \pm 0.04$	$4.93^d$
EW <sup>e</sup> (eV) .....	$38 \pm 16$	$<25$	$54 \pm 24$	$<46$
	$62 \pm 23$	$<21$	$69 \pm 37$	$<57$

<sup>a</sup> Photon index above 2 keV.

<sup>b</sup> 2–10 keV flux.

<sup>c</sup> Observed line energy.

<sup>d</sup> Model parameter is fixed in fit.

<sup>e</sup> Absorption-line equivalent width.

$\text{cm}^{-2} \text{s}^{-1}$  (at 1 keV). The integrated flux is  $1.42 \times 10^{-11}$  ergs  $\text{cm}^{-2} \text{s}^{-1}$  (0.4–8 keV), corresponding to an unabsorbed X-ray luminosity of  $2 \times 10^{44}$  ergs  $\text{s}^{-1}$ . The spectral fit obtained is formally unacceptable, with  $\chi^2/\text{dof} = 686/544$  (dof = degrees of freedom) for a rejection probability of  $2.9 \times 10^{-5}$ . This is due to several ionized emission and absorption lines (e.g., from O, Ne) below 1 keV, although the continuum is fitted well above 2 keV. A single-power-law model provides an adequate fit to the continuum above 2 keV, with a photon index of  $\Gamma = 1.99 \pm 0.06$ . The fit statistic obtained is  $\chi^2/\text{dof} = 116.4/93$ , which is marginally acceptable (the rejection probability is  $5 \times 10^{-2}$ ). Figure 1 shows the LETG counts spectrum above 2 keV, with the lower panel showing the  $\chi^2$  residuals of the data compared to the continuum model. Each bin represents the FWHM resolution of the LETG. Two strong negative deviations that contribute significantly toward the total  $\chi^2$  are observed near 4.2 and 4.9 keV, due to two absorption lines in the PG 1211+143 spectrum. To test this, two unresolved ( $\sigma = 10$  eV) Gaussian absorption lines were added to the continuum model. A significant improvement in the spectral fit was obtained ( $\chi^2/\text{dof} = 83.4/89$ ), with the addition of two ab-

sorption lines at  $4.22 \pm 0.03$  and  $4.93 \pm 0.03$  keV (observed frame) with equivalent widths of  $35 \pm 16$  and  $57 \pm 23$  eV, respectively. The improvement in the fit statistic upon adding each line was  $\Delta\chi^2 = 13.8$  and  $\Delta\chi^2 = 19.9$ , respectively, while the overall fit statistic is now acceptable.

To constrain the width of the two absorption lines, the LETG spectrum was rebinned to their maximum resolution, with each bin representing  $\frac{1}{4}$  FWHM resolution of the LETG ( $\Delta\lambda = 0.0125 \text{ \AA}$  or  $\Delta E = 16$  eV at 4 keV). The rest-frame spectrum at this resolution near the absorption lines is shown in Figure 2. The spectral fit was minimized using the C-statistic (Cash 1979), due to the lower number of counts per bin at this resolution. The best-fit width is  $\sigma \sim 21$  eV (at 4.9 keV), corresponding to an FWHM velocity of  $\sim 3000$   $\text{km s}^{-1}$ . However, the line width is poorly constrained, with the 90% upper limit being  $<7800$   $\text{km s}^{-1}$ . The variability of the absorption lines was tested by comparing the LETG spectra across all three *Chandra* orbits. The first LETG orbit was simultaneous with *XMM-Newton*, so the LETG and EPIC-pn spectra were fitted jointly. The results are shown in Table 1, while the C-statistic

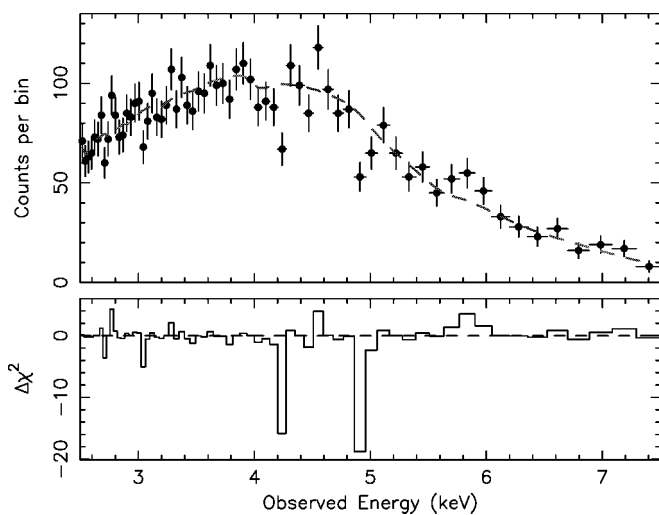


FIG. 1.—The upper panel shows the first-order *Chandra* LETG spectrum of PG 1211+143 above 2 keV; data points are shown as filled circles, and  $1 \sigma$  error bars as vertical lines. The best-fitting continuum model, folded through the LETG response, is shown as a dashed line. The spectrum has been binned to the FWHM LETG spectral resolution and is plotted in the observed frame. The lower panel plots the  $\chi^2$  residuals between the data and the continuum model; negative residuals correspond to a deficit of counts. Two absorption features are apparent at 4.2 and 4.9 keV, respectively.

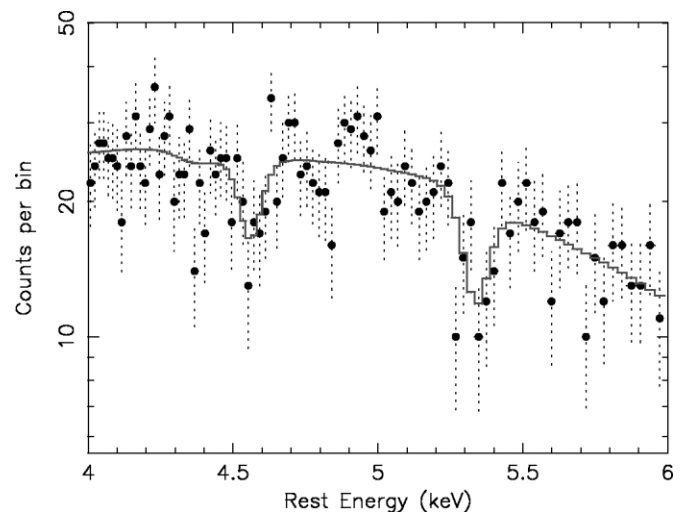


FIG. 2.—LETG spectrum of PG 1211+143 between 4 and 6 keV, binned at the full LETG resolution of  $\Delta\lambda = 0.0125 \text{ \AA}$  (equivalent to  $\frac{1}{4}$  FWHM resolution per bin). Data are shown as filled circles, with the dotted lines showing the  $1 \sigma$  error bars and the solid line showing the best-fit absorption-line model. The spectrum has been transformed into the rest frame of PG 1211+143. If identified with Fe xxvi K $\alpha$ , the redshift of each line would correspond to velocities of  $0.26c$  and  $0.40c$ . Note that the relative separation of the lines requires that two separate velocity components are present. [See the electronic edition of the *Journal* for a color version of this figure.]

was used to minimize the spectral fits. The 4.2 and 4.9 keV lines are only formally detected during the second orbit, although orbits 2 and 3 are statistically consistent. The lines do appear to vary in equivalent width between orbits 1 and 2 at >90% confidence.

### 3.1. Statistical Significance of the Absorption Lines

In order to check that the absorption is not due to calibration effects, the PG 1211+143 spectrum was compared to all the archived LETG observations of 3C 273. No residuals are present in the summed or individual 3C 273 spectra near the 4.22 and 4.93 keV line energies (Fig. 3). The limit on the equivalent width of any absorption lines is <4 eV in the summed spectrum. The source and background spectral extraction regions of PG 1211+143, in each of the three *Chandra* orbits, were also inspected. No anomalous pixels or rows were observed in the CCD array, and no background sources were present within the extraction regions. The separate  $\pm 1$  order spectra of PG 1211+143 were also found to be consistent. Thus, the lines are not due to systematic or calibration effects in the LETG.

In order to assess the statistical significance of the lines, we wish to determine the chance probability of falsely detecting two lines, over an energy band of interest. In order to estimate this, 1000 LETG spectra were simulated, under the null hypothesis assumption that the spectrum consists of a broken power-law continuum from 0.4 to 8.0 keV, with no spectral lines. The distribution of  $\Delta\chi^2$  values obtained by fitting a single Gaussian line to each of the 1000 spectra simulated in the null hypothesis case can then be compared to the measured  $\Delta\chi^2$  in the real data set to calculate the false probability of detection (Porquet et al. 2004). The first-order LETG spectra were simulated using identical continuum parameters and exposures as in the real PG 1211+143 data set and binned at the FWHM resolution of the LETG. A single narrow Gaussian line (in either absorption or emission) was added to the continuum model and then fitted to each simulated spectrum. The line energy was stepped in increments of 1 FWHM resolution bin over the 3–7 keV band, and the simulated spectrum was refitted at each increment to minimize  $\chi^2$ . The minimum  $\chi^2$  obtained from adding the line to the spectral fit was compared to the  $\chi^2$  obtained for the continuum model alone for each spectrum, in order to compute the distribution of  $\Delta\chi^2$  versus probability for all 1000 simulated spectra. The 3–7 keV band was chosen for the line search as it is most likely that a strong iron  $K\alpha$  line will be observed over this energy range; i.e., <3 keV is outside the iron K bandpass for any feasible redshift, while the LETG has little effective area above 7 keV. The improvement in the fit statistic obtained by adding the two lines to the actual data set was  $\Delta\chi^2 = 13.8$  and  $\Delta\chi^2 = 19.9$  for each line. The simulations show that the false probability of detecting a line with equal or greater  $\Delta\chi^2$  is 0.034 and 0.004 for the 4.2 and 4.9 keV lines, respectively. The probability of both lines being false detections is the product of these probabilities, which is  $1.36 \times 10^{-4}$ .

As an independent check, we calculate the line significances using the actual errors on the fitted parameters. The absorption-line fluxes at 4.2 and 4.9 keV are  $-(4.9 \pm 1.3) \times 10^{-6}$  and  $-(5.9 \pm 1.5) \times 10^{-6}$  photons  $\text{cm}^{-2} \text{s}^{-1}$ , respectively, while the continuum fluxes at these energies are  $(1.40 \pm 0.10) \times 10^{-4}$  and  $(1.04 \pm 0.08) \times 10^{-4}$  photons  $\text{cm}^{-2} \text{s}^{-1} \text{keV}^{-1}$ . The equivalent widths of the lines are then  $-35 \pm 10$  and  $-57 \pm 15$  eV, respectively. The errors are 1  $\sigma$  values, and the line flux and continuum errors have been propagated. Thus, the two absorption

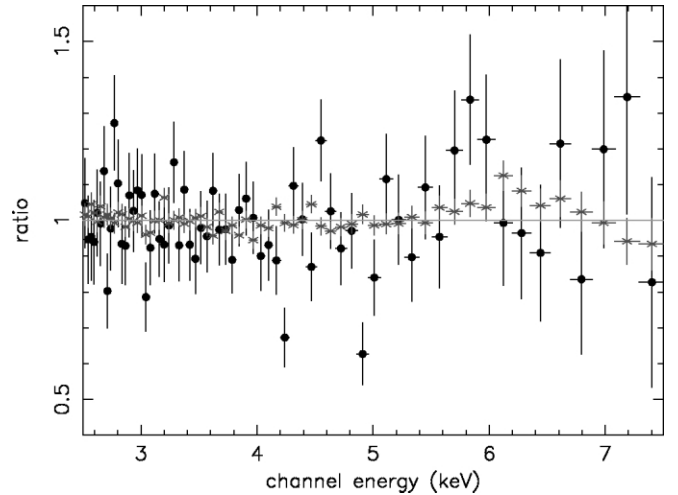


Fig. 3.—Data/model ratio residuals of the PG 1211+143 (circles) and 3C 273 (asterisks) LETG spectra to power-law continuum models fitted above 2 keV. The data were binned at the FWHM resolution of the LETG. The absorption lines apparent between 4 and 5 keV in PG 1211+143 do not appear in the 3C 273 spectrum, ruling out calibration effects. [See the electronic edition of the *Journal* for a color version of this figure.]

lines are significant at  $3.5 \sigma$  and  $3.8 \sigma$ , with corresponding null probabilities of  $4.6 \times 10^{-4}$  and  $1.4 \times 10^{-4}$ . However, these are single trial probabilities for a line at an a priori known energy. Taking into account the number of bins  $N$  searched for line features in the 3–7 keV range, then the null detection probability  $P$  will be  $P = 1 - (1 - P_1)^N$ , where  $P_1$  is the single trial probability from above. As there are 48 resolution bins in the 3–7 keV range, the null probabilities for the 4.2 and 4.9 keV lines are 0.022 and 0.0067 respectively, in agreement with the Monte Carlo estimates.

## 4. DISCUSSION

Although the lines are likely to be associated with redshifted Fe  $K\alpha$ , we first consider whether the lines could originate from other elements at lower velocities. The absorption-line rest-frame energies are  $4.56 \pm 0.03$  and  $5.33 \pm 0.03$  keV, respectively. The closest transitions to those energies are Sc xxI  $K\alpha$  (at 4.53 keV) or V xxIII (5.43 keV), respectively. The abundances of Sc or V are extremely low,  $\sim 1000$  times less than Fe. Even if the abundances were enhanced through spallation of iron nuclei by energetic protons on the disk surface (Skibo 1997), the strengths of these lines would still be considerably weaker ( $\ll 10\%$ ) than due to Fe  $K\alpha$ . One other possibility is that the absorption originates from lower  $Z$  elements such as Si, S, or Ca in a relativistic outflow. Blueshifted lines with  $v \sim 0.1c$  have been detected in PG 1211+143 in a previous *XMM-Newton* observation by Pounds et al. (2003). In this case, Ca xx at 4.10 keV would appear the most reasonable identification for the lower energy line, requiring an outflow velocity of  $32,000 \text{ km s}^{-1}$ . However, the Ca xx line is still likely to be weak, as the abundance ratio is  $\text{Fe}/\text{Ca} \sim 20$  (Anders & Grevesse 1989). Si or S is more abundant than Ca; however, if the lines originate from Si xiv  $K\alpha$  and S xvi  $K\alpha$ , then the outflow velocities are  $0.68c$  and  $0.62c$ , respectively. The kinetic power of such a fast flow would be a factor of  $\sim 40$  greater than calculated by Pounds et al. (2003), probably exceeding  $10^{46}$  ergs  $\text{s}^{-1}$  and the bolometric output of the quasar. Such a highly energetic flow seems implausible, unless the opening angle of the outflow is small.

The most likely scenario is that the lines originate from highly

redshifted iron  $K\alpha$ . Nandra et al. (1999) first claimed the possibility of redshifted iron K-shell absorption, through *ASCA* observations of the Seyfert 1 galaxy NGC 3516. However, recent *Chandra* and *XMM-Newton* observations (Turner et al. 2002) have showed that this is probably due to a strong narrow  $K\alpha$  core at 6.4 keV and variable emission lines at  $<6.4$  keV. Other claimed examples include a 6.2 keV line in the quasar 1E 1821+643 with the High Energy Transmission Grating on *Chandra* (Yaqoob & Serlemitsos 2005) and a weak redshifted line in the quasar Q0056–363 (Matt et al. 2005). Most recently, the detection of transient redshifted Fe absorption lines in Mrk 509 was claimed in *BeppoSAX* data, with a velocity shift of  $v = 0.21c$  (Dadina et al. 2005).

If the lines in PG 1211+143 correspond to H-like iron (i.e., Fe xxvi  $K\alpha$  at 6.97 keV), then the redshifted velocities are  $0.26c$  and  $0.40c$ , while if the lines correspond to He-like iron (Fe xxv  $K\alpha$  resonance at 6.70 keV), the velocities are  $0.22c$  and  $0.37c$ . Note that the separation of the two lines requires two distinct velocity components, as the higher order Fe  $K\beta$  lines are undetectable in this spectrum. It is unlikely that the lines result from a lower ionization than Fe xxv, as then a series of strong L-shell Fe lines and edges would be detected at lower energies, which is not the case. Furthermore, the absorption lines cannot be from near-neutral Fe (Fe I–VII) at 6.4 keV, because no strong  $K\alpha$  absorption line would be observed, as the L shell would be fully populated.

The two possible causes for the relativistic shifts are either gravitational redshift of photons near the massive black hole or infall of matter onto the black hole. In the former scenario, the absorbing matter would have to be located at  $(3.5 \pm 0.5)R_g$  and  $(4.8 \pm 0.5)R_g$ , respectively, from a Schwarzschild black hole (where  $R_g = GM/c^2$  is 1 gravitational radius). This is within the last stable orbit around a Schwarzschild black hole and requires a Kerr metric (Thorne 1974) for the matter to exist in a stable orbit within  $6R_g$ . For a maximal pole-on Kerr black hole, the radii derived are then  $3.2R_g$  and  $4.6R_g$ , respectively. Alternatively, the matter may be infalling onto the black hole, in which case a maximum velocity of  $\sim 0.38c$  (in the frame of the observer) can be achieved at  $6R_g$  for a Schwarzschild metric.

Modeling the two absorption-line systems with XSTAR (Kallman et al. 1996) requires a large column density of  $N_H = 4.0^{+3.7}_{-1.9} \times 10^{23} \text{ cm}^{-2}$  (assuming a turbulence of  $\sigma_v = 1000 \text{ km s}^{-1}$  and solar abundances). The ionization parameter is  $\log \xi = 3.9 \pm 0.3 \text{ ergs cm s}^{-1}$ , with most of the absorption arising from Fe xxvi  $K\alpha$ . The equivalent column density of

Fe xxvi is  $\sim 7 \times 10^{18} \text{ cm}^{-2}$ , while the optical depth at the K-shell edge is  $\tau < 0.1$ ; i.e., the matter is optically thin to the continuum. The velocity of the two absorption systems are  $v = (0.28 \pm 0.01)c$  and  $v = (0.42 \pm 0.01)c$ , while the line-of-sight covering fraction is  $>50\%$ . From the above parameters, we can derive the physical properties of the gas. A black hole mass of  $4 \times 10^7 M_\odot$  is assumed (Kaspi et al. 2000), along with an ionizing luminosity of  $L \sim 10^{44} \text{ ergs s}^{-1}$  and a radial distance of  $R \sim 10^{14} \text{ cm}$  (i.e., a few  $R_g$ ). The ionization parameter is defined as  $\xi = L/nR^2$  ( $n$  is the electron density), while one can define a filling factor  $f$  as  $f = \Delta R/R = N_H/nR$ . A density of  $n \sim 10^{12} \text{ cm}^{-3}$  is calculated, with a filling factor of  $\sim 1\%$  and a cloud size of  $\sim 10^{12} \text{ cm}$ . Note that these should be considered order-of-magnitude estimates, due to the uncertainties in  $R$  and black hole mass.

A fast outflow of  $\sim 0.1c$  has already been detected in an earlier *XMM-Newton* observation of PG 1211+143 (Pounds et al. 2003), which is confirmed from the analysis of the soft X-ray LETG data (J. N. Reeves et al. 2005, in preparation). One possibility is that part of this outflow does not escape the gravitational potential of the black hole (Murray & Chiang 1998; Proga et al. 2000). If material is launched with  $v = 0.1c$  in PG 1211+143, then matter within a radius of  $R < 100R_g$  may not escape the system. Thus, it is possible to produce both red- and blueshifted lines in PG 1211+143; indeed, in Mrk 509, both inflow and outflow also appear to be present (Dadina et al. 2005). From above, the mass infall rate required is  $\dot{M} \sim \pi f n R^2 v m_p \sim \pi L v f m_p / \xi \sim 10^{25} \text{ g s}^{-1}$  or  $\sim 0.1 M_\odot \text{ yr}^{-1}$ . The kinetic power is then a few times  $10^{44} \text{ ergs s}^{-1}$  for an infall velocity of  $v = c/3$ . Interestingly, this is similar to the X-ray luminosity of PG 1211+143. Indeed, a similar ‘‘aborted jet’’ model has been proposed by Ghisellini et al. (2004), where matter in an outflow or jet fails to escape the gravitational potential well.

Alternatively, the absorption may originate from matter near the highly ionized inner disk surface, with the redshift being largely gravitational in origin. Ruszkowski & Fabian (2000) proposed such a model to explain the absorption line in NGC 3516, although the lines will be broad unless the matter is clumped. Monitoring the line variability will help us to reveal its origin; for instance, it may be possible to track the infall of a dense clump of matter toward the black hole. Regardless of the mechanism, the large redshift and high covering fraction imply that most of the X-ray emission in PG 1211+143 originates from a compact region within a few  $R_g$  of the black hole.

#### REFERENCES

- Anders, E., & Grevesse, N. 1989, *Geochim. Cosmochim. Acta*, 53, 197  
 Cash, W. 1979, *ApJ*, 228, 939  
 Dadina, M., Cappi, M., Malaguti, G., Ponti, G., & De Rosa, A. 2005, *A&A*, in press  
 Dickey, J. M., & Lockman, F. J. 1990, *ARA&A*, 28, 215  
 Dovciak, M., Bianchi, S., Guainazzi, M., Karas, V., & Matt, G. 2004, *MNRAS*, 350, 745  
 Fabian, A. C., Rees, M. J., Stella, L., & White, N. E. 1989, *MNRAS*, 238, 729  
 Ghisellini, G., Haardt, F., & Matt, G. 2004, *A&A*, 413, 535  
 Kallman, T. R., Liedahl, D., Osterheld, A., Goldstein, W., & Kahn, S. 1996, *ApJ*, 465, 994  
 Kaspi, S., Smith, P. S., Netzer, H., Maoz, D., Jannuzi, B. T., & Giveon, U. 2000, *ApJ*, 533, 631  
 Laor, A. 1991, *ApJ*, 376, 90  
 Matt, G., Porquet, D., Bianchi, S., Falocco, S., Maiolino, R., Reeves, J. N., & Zappacosta, L. 2005, *A&A*, 435, 857  
 Murray, N., & Chiang, J. 1998, *ApJ*, 494, 125  
 Nandra, K., George, I. M., Mushotzky, R. F., Turner, T. J., & Yaqoob, T. 1997, *ApJ*, 477, 602  
 Nandra, K., George, I. M., Mushotzky, R. F., Turner, T. J., & Yaqoob, T. 1999, *ApJ*, 523, L17  
 Porquet, D., Reeves, J. N., Uttley, P., & Turner, T. J. 2004, *A&A*, 427, 101  
 Pounds, K. A., Reeves, J. N., King, A., Page, K., O’Brien, P. T., & Turner, M. J. L. 2003, *MNRAS*, 345, 705  
 Proga, D., Stone, J. M., & Kallman, T. R. 2000, *ApJ*, 543, 686  
 Reeves, J. N., Nandra, K., George, I. M., Pounds, K. A., Turner, T. J., & Yaqoob, T. 2004, *ApJ*, 602, 648  
 Ruszkowski, M., & Fabian, A. C. 2000, *MNRAS*, 315, 223  
 Skibo, J. G. 1997, *ApJ*, 478, 522  
 Tanaka, Y., et al. 1995, *Nature*, 375, 659  
 Thorne, K. S. 1974, *ApJ*, 191, 507  
 Turner, T. J., Kraemer, S. B., George, I. M., Reeves, J. N., & Bottorff, M. C. 2005a, *ApJ*, 618, 155  
 Turner, T. J., Miller, L., George, I. M., & Reeves, J. N. 2005b, *A&A*, in press  
 Turner, T. J., et al. 2002, *ApJ*, 574, L123  
 Yaqoob, T., & Padmanabhan, U. 2004, *ApJ*, 604, 63  
 Yaqoob, T., & Serlemitsos, P. 2005, *ApJ*, 623, 112